

PAPER • OPEN ACCESS

All-optical spatio-temporal control of electron emission from SiO₂ nanospheres with femtosecond two-color laser fields

To cite this article: Qingcao Liu *et al* 2019 *New J. Phys.* **21** 073011

View the [article online](#) for updates and enhancements.

Recent citations

- [Interplay of pulse duration, peak intensity, and particle size in laser-driven electron emission from silica nanospheres](#)
Jeffrey A. Powell *et al*



PAPER

All-optical spatio-temporal control of electron emission from SiO₂ nanospheres with femtosecond two-color laser fields

OPEN ACCESS

RECEIVED

13 March 2019

REVISED

13 May 2019

ACCEPTED FOR PUBLICATION

4 June 2019








PUBLISHED

1 July 2019

Original content from this work may be used under the terms of the [Creative Commons Attribution 3.0 licence](https://creativecommons.org/licenses/by/4.0/).

Any further distribution of this work must maintain attribution to the author(s) and the title of the work, journal citation and DOI.



Qingcao Liu^{1,2} , Sergey Zhrebtsov^{1,2}, Lennart Seiffert³ , Slawomir Skruszewicz³, Dominik Zietlow^{1,2}, Seongjin Ahn^{4,5}, Philipp Rupp², Pawel Wnuk^{1,2}, Shaohua Sun², Alexander Kessel^{1,2}, Sergei Trushin^{1,2}, Annika Schlander⁶, Dongeon Kim^{4,5}, Eckart Rühl⁷ , Marcelo F Ciappina⁸ , Josef Tiggesbäumker³, Markus Gallei^{6,9} , Thomas Fennel^{3,10}  and Matthias F Kling^{1,2} 

¹ Max Planck Institute of Quantum Optics, D-85748 Garching, Germany

² Physics Department, Ludwig-Maximilians-Universität Munich, D-85748 Garching, Germany

³ Institute of Physics, University of Rostock, D-18051 Rostock, Germany

⁴ Department of Physics and Center for Attosecond Science and Technology, Pohang University of Science and Technology, Pohang, Gyeongbuk 37673, Republic of Korea

⁵ Max Planck POSTECH/KOREA Res. Init., Pohang, Gyeongbuk 37673, Republic of Korea

⁶ Macromolecular Chemistry Department, Technische Universität Darmstadt, D-64287 Darmstadt, Germany

⁷ Physical Chemistry, Freie Universität Berlin, Arnimallee 22, D-14195 Berlin, Germany

⁸ Institute of Physics of the ASCR, ELI-Beamlines project, Na Slovance 2, 18221 Prague, Czech Republic

⁹ Organic and Macromolecular Chemistry, Saarland University, D-66123 Saarbrücken, Germany

¹⁰ Max-Born-Institut, Max-Born-Straße 2 A, D-12489 Berlin, Germany

E-mail: matthias.kling@lmu.de

Keywords: ultrafast nanophysics, two-color laser fields, spatio-temporal control, dielectric nanospheres

Abstract

Field localization by nanostructures illuminated with laser pulses of well-defined waveform enables spatio-temporal tailoring of the near-fields for sub-cycle control of electron dynamics at the nanoscale. Here, we apply intense linearly-polarized two-color laser pulses for all-optical control of the highest energy electron emission from SiO₂ nanoparticles. For the size regime where light propagation effects become important, we demonstrate the possibility to control the preferential emission angle of a considerable fraction of the fastest electrons by varying the relative phase of the two-color field. Trajectory based semi-classical simulations show that for the investigated nanoparticle size range the directional steering can be attributed to the two-color effect on the electron trajectories, while the accompanied modification of the spatial distribution of the ionization rate on the nanoparticle surface has only a minor effect.

1. Introduction

Intense laser pulses with tailored waveforms have proven to be a powerful tool for the control of electron dynamics in atomic, molecular, and solid targets [1–12]. The laser electric field of such pulses exerts a force that varies on the attosecond time scale for visible light and enables the steering of electron motion on sub-cycle time scales and on nanometer spatial dimensions or even below [13–17]. In case of nanostructured materials, the spatial variation of the strongly localized optical near-field provides an additional control parameter for both electron emission and acceleration [17–20]. The coherent control of electron emission and acceleration with carrier-envelope phase (CEP)-controlled few-cycle laser pulses has been investigated for isolated nanospheres [19, 21–23], metal nanotips [24, 25], and surface assembled nanostructures [26–28]. Characteristic nanoscale phenomena that contribute to the strong-field photoemission from these materials include (i) the transition from ponderomotive to sub-cycle electron acceleration for field localization below the scale of the electron quiver motion [29], and (ii) field propagation induced directionality of the energetic electron emission as demonstrated for nanospheres with diameters approaching the wavelength of the incident light [19].

Here, we extend the near-field control of the photoemission from nanospheres to the multi-color regime. We demonstrate that spatio-temporal tailoring of the near-field with the two-color phase enables all-optical

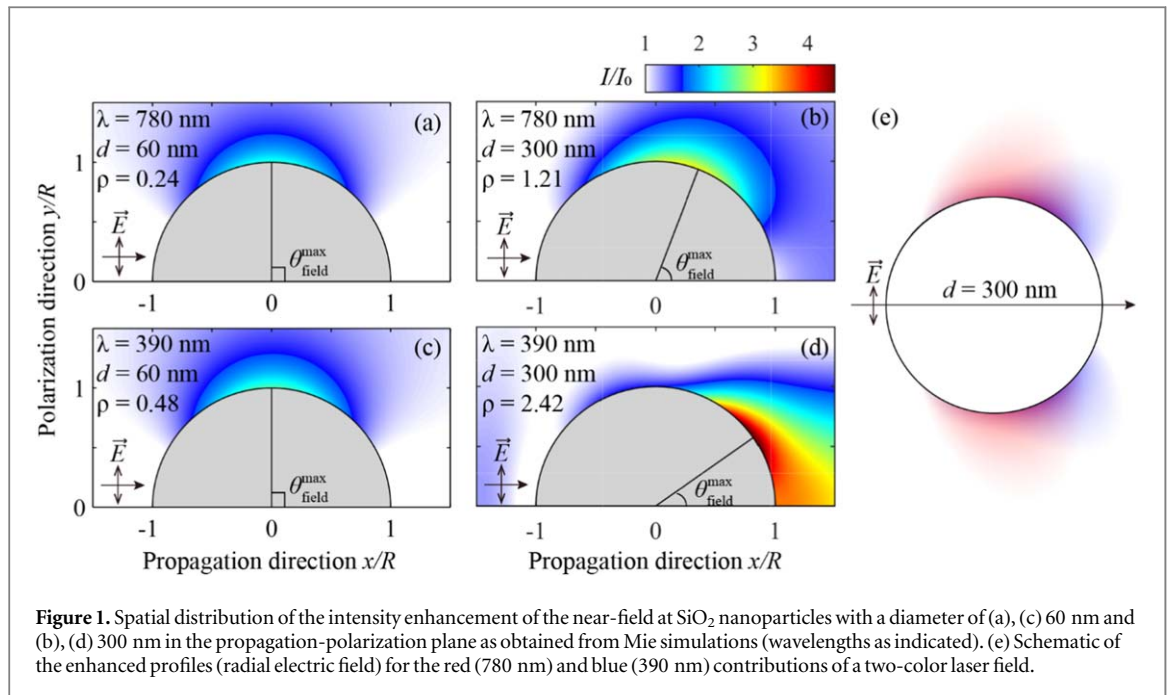


Figure 1. Spatial distribution of the intensity enhancement of the near-field at SiO₂ nanoparticles with a diameter of (a), (c) 60 nm and (b), (d) 300 nm in the propagation-polarization plane as obtained from Mie simulations (wavelengths as indicated). (e) Schematic of the enhanced profiles (radial electric field) for the red (780 nm) and blue (390 nm) contributions of a two-color laser field.

control of the electron emission direction. The waveform of the combined two-color driving field $E(t) = E_{\omega}(t)[\cos(\omega t) + \sqrt{\eta} \cos(2\omega t + \varphi_r)]$ depends on the relative phase φ_r , and the intensity ratio $\eta = I_{2\omega}/I_{\omega}$. The linear response of a nanoparticle to laser light can be accurately described by the Mie solution of Maxwell's equations. For a sphere with diameter d subjected to an incident field with wavelength λ , the impact of propagation effects on the near-field distribution can be characterized by the dimensionless Mie parameter $\rho = \pi d/\lambda$. For nanoparticles much smaller than the wavelength of the laser field ($\rho \ll 1$), the near-field distribution shows a dipole-like character with maximum field enhancement along the laser polarization direction (figures 1(a), (c)). As the size of a nanoparticle becomes sufficiently large with an associated Mie parameter $\rho > 1$, see figures 1(b), (d), excitation of higher order multipole modes results in a shift of the region of maximal field enhancement in the direction of light propagation. Thus, for an appropriately sized nanoparticle illuminated with linearly-polarized two-color laser pulses consisting of the fundamental wave and its second harmonic ($\omega/2\omega$ pulses), the near-field distributions of the ω and 2ω spectral components exhibit different spatial near-field profiles and, most importantly, the points of maximum enhancement (hot spots) are spatially separated. This is illustrated in figure 1 for a 300 nm diameter SiO₂ sphere, where the distributions of the near-field enhancement differ significantly for excitation with the fundamental (figure 1(b)) and the second harmonic (figure 1(d)) fields at 780 nm and 390 nm, respectively, and evidenced by the angle $\theta_{\text{field}}^{\text{max}}$, where maximum enhancement is observed. The fact that both the positions and extensions of the hot spots differ substantially for the two spectral field components (as depicted in figure 1(e)) motivates the possibility of all-optical control of the directionality of the near-cutoff electron emission. In this study, we demonstrate feasibility of this idea and explore how tailoring of the temporal waveform of the incident two-color field via its relative phase φ_r and intensity ratio η translates into modifications of the angular distributions of the yield and maximal energy of electrons.

2. Results and discussion

The experimental setup for velocity-map imaging (VMI) of the electron emission is shown in figure 2(a). A beam of isolated SiO₂ nanoparticles was prepared via an aerosol technique [30], where the particles were brought into a gas stream of N₂ from suspension in ethanol, dried out by a diffusion dryer and focused into the laser focus with an aerodynamic lens, after which most of the residual gas was removed through differential pumping [17, 20–23]. Silica nanoparticles with diameters of 60 and 300 nm and a narrow size distribution were prepared by wet chemistry approaches. Firstly, small seed nanoparticles were prepared by the Stöber method [31]. In a typical seed preparation procedure 21 g of TEOS, 28 ml of ammonia solution (25 wt% in water) and 1 ml of water were added to 530 ml of ethanol and stirred for 12 h. Further shells were grown on the silica nanoparticles successively by the seeded growth method [32] until the desired particle size was reached. All samples have been stored in ultrapure ethanol after cleaning. Characterization by transmission electron microscopy as well as dynamic light scattering yielded a polydispersity of about 5% for the 60 nm and 2.9% for the 300 nm particles, respectively.

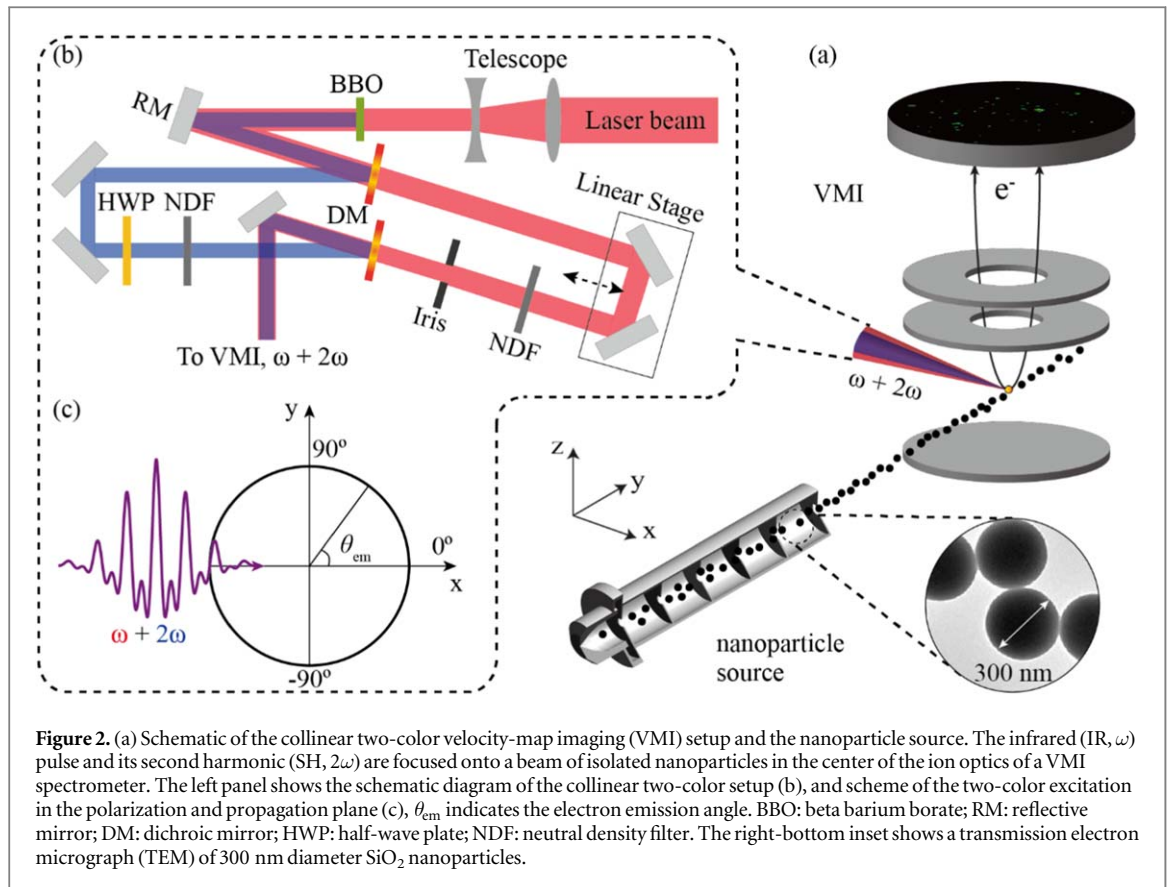


Figure 2(b) shows the schematic diagram of the collinear two-color setup. The infrared (IR, ω) laser pulses of 30 fs duration centered at 780 nm at 1 kHz repetition rate with an energy of up to 1.3 mJ were obtained from an amplified Ti:Sapphire laser system (see [33, 34] for details). The laser beam was sent into a telescope (2:1) before entering a BBO crystal, where a second harmonic (SH, 2ω) pulse was generated with polarization orthogonal to the fundamental. Both pulses were sent into a Mach-Zehnder interferometer to generate delay-controlled two-color pulses. The polarization of the SH pulse was rotated by 90° via a half-wave plate and became parallel to that of the IR pulse. To match the spatial intensity profiles of the 2ω and ω pulses in the focus, an iris was introduced into the IR arm of the interferometer. The intensities of the ω and 2ω components were controlled by neutral density filters in both arms. The resulting laser pulses were focused with a 50 cm focal length mirror and intersected the nanoparticle beam in the center of the ion optics of a VMI spectrometer. The electron emission was projected onto a micro-channel-plate (MCP)/phosphor screen assembly and the resulting image was recorded for each laser shot with a complementary-metal-oxide-semiconductor camera [35]. The discrimination of the single-shot frames to those that contain emitted electrons from aerosolized nanoparticles is performed by selecting frames with more than 30 electrons, where the typical number of detected electrons from the background gas is less than 20 in this study.

The scheme of the two-color excitation in the polarization-propagation plane is depicted in figure 2(c). In the experiment, the field waveform was precisely controlled by a computer-controlled linear translation stage in one of the interferometer arms. The laser parameters in the interaction volume such as intensity and relative two-color phase were determined from reference measurements of above-threshold ionization (ATI) of xenon and comparison to time-dependent Schrödinger equation simulations [36].

The effect of the two-color field on the electron photoemission and acceleration was studied for SiO₂ nanospheres of two different diameters d : 60 and 300 nm, where electron emission was recorded as a function of the two-color phase. Figures 3(a), (f) show typical phase-averaged momentum distributions for both nanoparticle sizes. Although, at low momenta, the distributions may contain spurious photoemission signal from residual background gas, the high momentum electrons originate predominantly from nanoparticles via ionization and backscattering at the surface [19]. The high-energy signal can thus serve to inspect the directional control of the two-color electron emission. Figures 3(b), (c) and (g), (h) display typical phase-resolved VMI images after subtraction of the phase averaged spectra and reveal that a part of the electron emission can be effectively switched between the upwards or downwards direction.

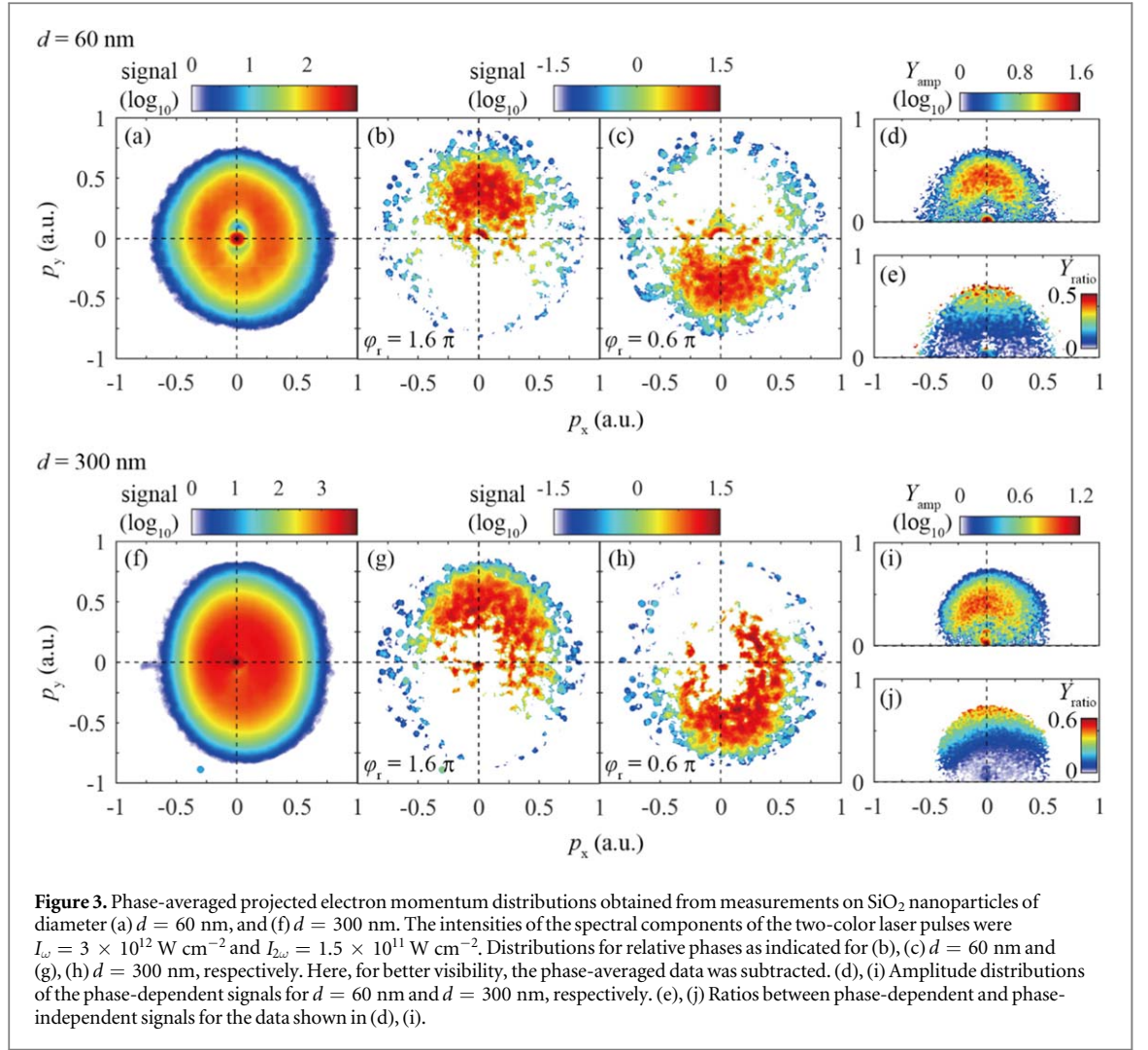


Figure 3. Phase-averaged projected electron momentum distributions obtained from measurements on SiO₂ nanoparticles of diameter (a) $d = 60$ nm, and (f) $d = 300$ nm. The intensities of the spectral components of the two-color laser pulses were $I_{\omega} = 3 \times 10^{12}$ W cm⁻² and $I_{2\omega} = 1.5 \times 10^{11}$ W cm⁻². Distributions for relative phases as indicated for (b), (c) $d = 60$ nm and (g), (h) $d = 300$ nm, respectively. Here, for better visibility, the phase-averaged data was subtracted. (d), (i) Amplitude distributions of the phase-dependent signals for $d = 60$ nm and $d = 300$ nm, respectively. (e), (j) Ratios between phase-dependent and phase-independent signals for the data shown in (d), (i).

In order to investigate more quantitatively, which portion of the emitted high-energy electrons can be controlled by the two-color phase in the experiments, we have extracted the phase-dependent and -independent electron yields by fitting the data for each momentum with the function $Y(p_x, p_y, \varphi_r) = Y_{\text{amp}}(p_x, p_y) \cos(\varphi_r + \Delta\varphi(p_x, p_y)) + Y_{\text{indep.}}(p_x, p_y)$ where $Y_{\text{amp}}(p_x, p_y)$ is the amplitude of the phase-dependent signal, $\Delta\varphi(p_x, p_y)$ is a phase offset, and $Y_{\text{indep.}}(p_x, p_y)$ is the phase-independent signal. The amplitudes of the phase-dependent signals are shown in figures 3(d), (i) for $d = 60$ nm and $d = 300$ nm, respectively. To illustrate the degree of control, the ratios between the phase-dependent and -independent signals $Y_{\text{ratio}}(p_x, p_y) = Y_{\text{amp}}(p_x, p_y) / Y_{\text{indep.}}(p_x, p_y)$ were evaluated and are shown in figures 3(e), (j) for the data from figures 3(d), (i). We find that the ratio exceeds 0.5 in the near-cutoff regions, indicating a large degree of control with the phase of the two-color laser field.

For 60 nm diameter particles, field propagation effects are small for both spectral components of the two-color field ($\rho_{\omega} = 0.26$, $\rho_{2\omega} = 0.52$) such that the electron emission exhibits a directionally undistorted character with respect to the propagation direction, and a phase controlled contribution that is centered around angles of $\pm 90^\circ$. For the larger nanoparticles (300 nm), field propagation (in particular strong for the 2ω -component, see figure 1(d)) results in a substantial distortion of the electron distribution with an emission preference of high energy electrons towards angles being significantly smaller than 90° (tilted to the backside of the nanosphere) as shown in figures 3(g), (h).

While similar propagation-induced directional control of the electron emission has already been observed with CEP-controlled few-cycle pulses [19, 37], those studies have been carried out at a single (central) wavelength, such that a change of the CEP allowed only for control of the up versus down emission, while the directionality could only be steered by changing the particle size. In the present study, we focus on an all-optical control of the emission angle, where in addition to having two distinct fields controlled via the two-color phase, the intensity ratio provides an extra parameter to control the relative strength of propagation induced asymmetry in the electron emission in single-size nanoparticles (shown here for 300 nm). It is noteworthy that

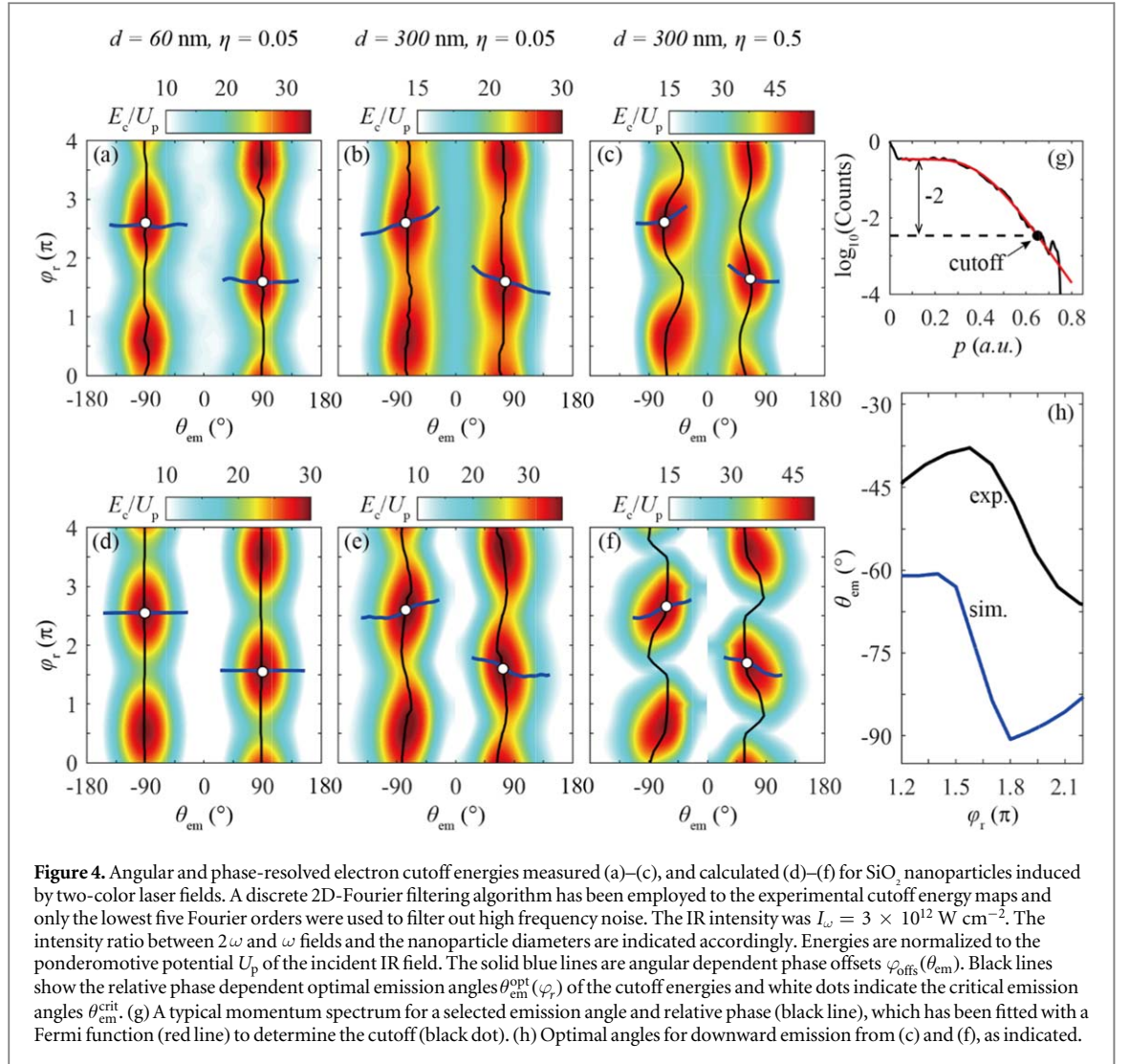


Figure 4. Angular and phase-resolved electron cutoff energies measured (a)–(c), and calculated (d)–(f) for SiO₂ nanoparticles induced by two-color laser fields. A discrete 2D-Fourier filtering algorithm has been employed to the experimental cutoff energy maps and only the lowest five Fourier orders were used to filter out high frequency noise. The IR intensity was $I_\omega = 3 \times 10^{12}$ W cm⁻². The intensity ratio between 2ω and ω fields and the nanoparticle diameters are indicated accordingly. Energies are normalized to the ponderomotive potential U_p of the incident IR field. The solid blue lines are angular dependent phase offsets $\varphi_{\text{offs}}(\theta_{\text{em}})$. Black lines show the relative phase dependent optimal emission angles $\theta_{\text{em}}^{\text{opt}}(\varphi_r)$ of the cutoff energies and white dots indicate the critical emission angles $\theta_{\text{em}}^{\text{crit}}$. (g) A typical momentum spectrum for a selected emission angle and relative phase (black line), which has been fitted with a Fermi function (red line) to determine the cutoff (black dot). (h) Optimal angles for downward emission from (c) and (f), as indicated.

our studies are carried out at intensities of several TW cm⁻², which are below the plasma generation threshold. The nanoparticles therefore remain intact during their interaction with the two-color field, such that the dynamics differs strongly from related works on the control of charged particle emission from clusters and nanoparticles in the plasma regime [36, 38].

The results of the phase-dependent measurements are presented in figures 4(a)–(c). The maps reflect the cutoff energy of photoemitted electrons as function of emission angle and relative ω - 2ω phase. Figure 4(g) shows a typical momentum spectrum for a selected emission angle and relative phase (black line) obtained from the measurement and fitted with a Fermi function (red line). The cutoff is obtained as the momentum where the corresponding normalized yield drops by two orders of magnitude compared to the yield in the plateau region. To quantify the two-color control of the photoemission, we perform two complementary analyses.

First, similar to the analysis of CEP-dependent emission in earlier work [24], the phase dependent electron cutoff energy E_c for each emission angle θ_{em} is fitted with a function $E_c = E_0 + E_{\text{amp}} \cos(\varphi_r - \varphi_{\text{offs}})$. Here, E_0 is a constant offset, E_{amp} is the maximum amplitude of the cutoff modulation and φ_{offs} is the relative phase for which the maximal cutoff is realized for a given angle. The emission angle which yields the maximum cutoff energy is called critical emission angle $\theta_{\text{em}}^{\text{crit}}$. The obtained angular dependent phase offsets $\varphi_{\text{offs}}(\theta_{\text{em}})$ and critical emission angles $\theta_{\text{em}}^{\text{crit}}$ are plotted as solid blue lines and white dots in figure 4, respectively. For the small nanoparticles (figure 4(a)), the critical emission angle is close to $\pm 90^\circ$, reflecting maximum enhancement at the particle poles in the absence of propagation effects for both ω and 2ω components. Note, that we find similar and therefore consistent behavior for small nanoparticles also for higher intensity ratios (not shown here). As a result, the relative phase has negligible effect on the directionality and only modulates the cutoff, with opposite sign for the upward versus downward emission direction. This type of directional control via the phase corresponds to the up-down switching observed previously with CEP-controlled few-cycle fields [19]. For the larger particles (figures 4(b)–(c)), however, the critical emission angle is not only shifted to smaller values

(i.e. towards the light propagation direction), as also seen in few-cycle experiments [19], but exhibits a clear structural modification of the angular distributions as a function of the relative ω - 2ω phase φ_r .

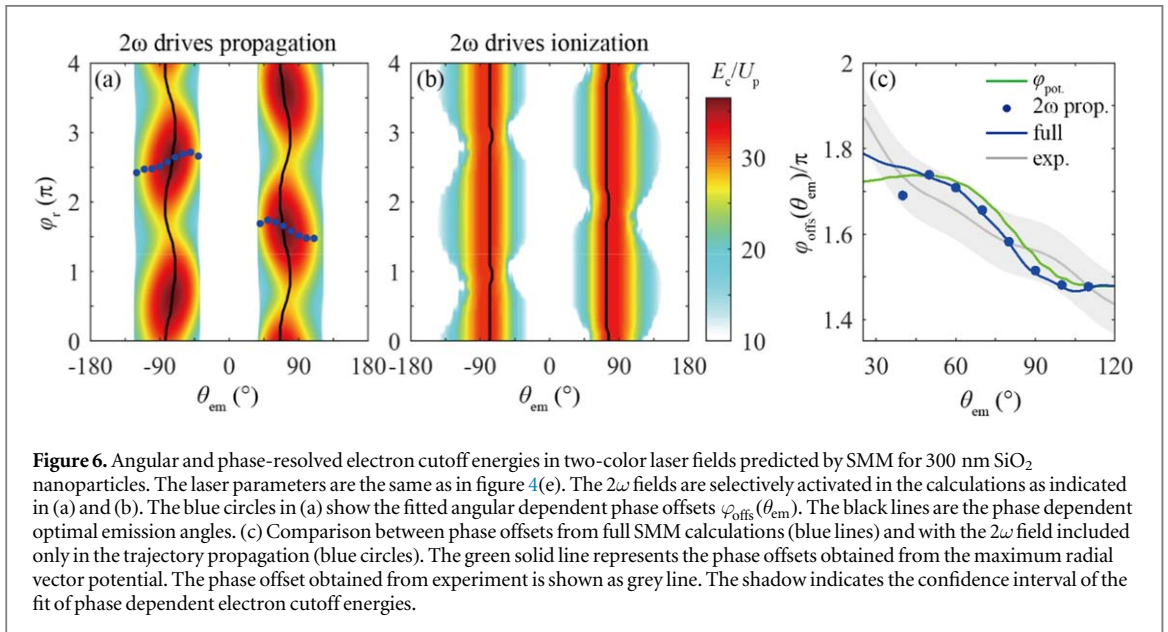
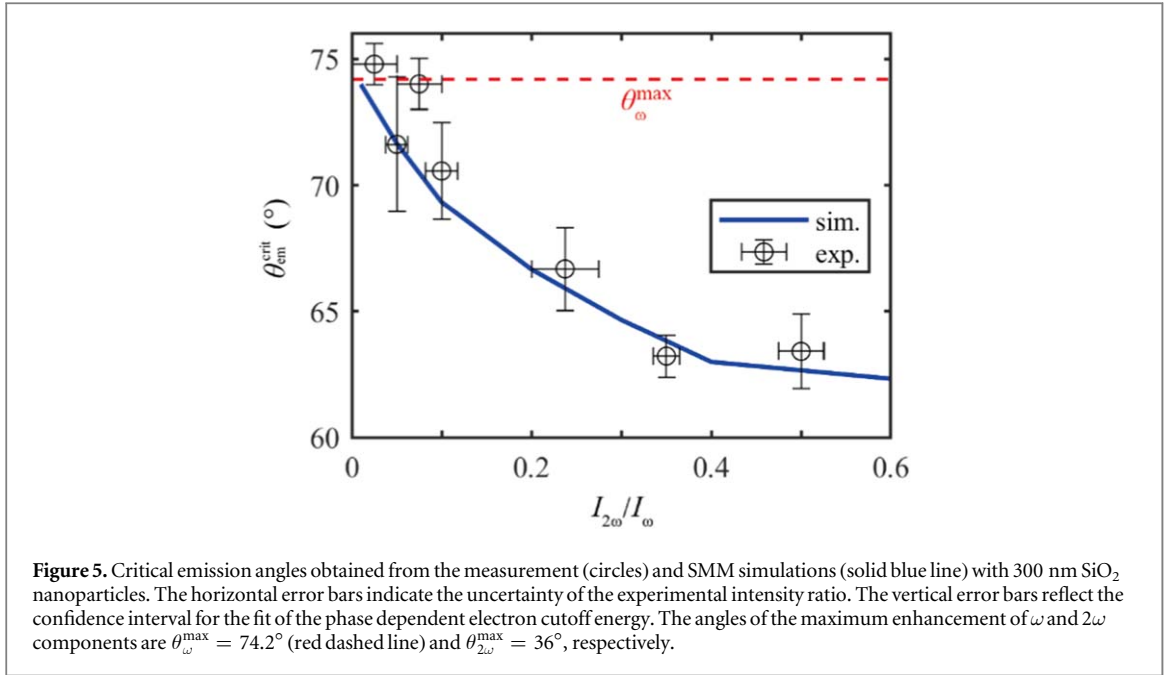
Second, to quantify the dynamics of the phase-dependent emission directionality, we inspect the optimal emission angle $\theta_{\text{em}}^{\text{opt}}(\varphi_r)$, which we define via the maximal energy of the emission in up/downward direction for each individual phase, see black curves in figure 4. For 300 nm nanoparticles, when the intensity ratio $I_{2\omega}/I_\omega$ is relatively small ($\eta = 0.05$), the optimal angle shows little variation around the critical emission angle $\theta_{\text{em}}^{\text{crit}} = 75^\circ$ (figure 4(b)). For a significantly larger intensity ratio ($\eta = 0.5$), the optimal angles are shifted to considerably smaller values and lie around 63° , see figure 4(c). Most importantly, they show a rapid variation (directional switching) of around 25° – 30° as function of the relative phase, see black curve in figure 4(h). These results demonstrate the feasibility of using two-color laser fields for the control of the emission direction of the most energetic electrons from nanoparticles. This observation goes beyond the recently shown two-color control of the cutoff in the electron emission from metallic nanotips [3, 4, 39].

To identify the mechanism behind the observed all-optical control of emission directionality of the most energetic electrons from nanospheres, we performed 3-dimensional semi-classical trajectory simulations based on the Simple-Man's Model (SMM) [40]. Briefly, classical electron trajectories are generated at the nanosphere surface and propagated in the two-color near-field. The temporal and spatial evolution of the latter is described by the Mie solution. For trajectories returning to the surface, elastic specular reflection is assumed. The energy acquired by the electron can be expressed in terms of the ponderomotive potential $U_p = \frac{e^2 E^2}{4m\omega^2} \sim I\lambda^2$, where e is the elementary charge, m the electron mass, E the amplitude, ω the laser frequency, λ the wavelength, and I the intensity of the ω component of the driving field. The trajectories are launched at the classical tunnel exit with zero velocity, and weighted by Ammosov–Delone–Krainov (ADK) atomic tunnel ionization rates [41]. As is known from previous work [21, 24, 29, 42], the near-field enhancement and multi-particle charge interaction of the liberated electrons and residual ions contribute to the electron acceleration process and can result in an increase of the electron emission cut-off to several tens of U_p [19, 21]. As the laser intensity in this study, however, was below $1 \times 10^{13} \text{ W cm}^{-2}$, where multi-electron effects are negligible [17], the SMM can provide an adequate description of the electron acceleration dynamics. The control of the photoemission of the most energetic electrons for small and large diameter SiO_2 nanoparticles, see figures 4(a)–(c), is well reproduced by the SMM simulations using the experimental parameters, see figures 4(d)–(f). Most importantly, the simplified model qualitatively reproduces the relative phase-dependent directional switching (see blue curve in figure 4(h)) in the relative phase region around the minimum cutoff energy for emission into the lower half space, see figures 4(c), (f). Due to the propagation induced retardation effects, the minimum cutoff energy is realized for different relative phases as function of angle—forming the physical grounds for the envisaged phase-controlled modification of the surface regions delivering the highest electron cutoff energy. The observed ‘drop feature’ is the most important qualitative signature that evidences the resulting switching. The remaining offset and the difference in the detailed oscillatory behavior in figure 4(h) are attributed to the simplicity of the SMM model that uses specular scattering. Nevertheless, the main qualitative feature is clearly captured by the model.

A quantitative analysis of the influence of the intensity ratio between the ω and 2ω components on the preferential energetic electron emission direction is presented in figure 5. The critical emission angle $\theta_{\text{em}}^{\text{crit}}$ starts at the angle of the maximum enhancement of the ω component $\theta_\omega^{\text{max}}$, and becomes smaller as the 2ω intensity increases. It shifts by about 10° when increasing the intensity from 0.05 to 0.5 I_ω . The results are quantitatively reproduced by our SMM simulations (blue line).

In principle, the presence of the 2ω field component can affect both the magnitude and spatial distribution of the ionization rate as well as the trajectory dynamics of the released electrons. The relative contributions of the effects of the 2ω field on the ionization rate and the trajectory propagation can be revealed by performing a selective activation in the SMM simulations, in analogy to the analysis in [4]. In figure 6 we show (a) the predicted angular and phase-resolved electron cutoff energies with the 2ω field included in the trajectory propagation but neglected in the ionization rate (here just driven by the ω field) and (b) for the 2ω field included in the ionization process, but propagation just driven by the ω field. Note that the impact on the tunnel exit is assumed to be negligible due to the relatively weak 2ω field. We closely compared the phase offsets from the calculations for both cases to the full simulation in figure 6(c). The phase offset from the full simulation (blue line) is well reproduced when including the 2ω component only in the propagation but not in the ionization (see blue circles).

Previous work has indicated that the radial fields on the nanoparticle surface were dominating the electron acceleration process [19]. To verify that this is also the case for the two-color control, we have inspected the phase evolution of the maximum radial vector potential (φ_{pot}) on the surface. The very good agreement with the experimental and full two-color simulation data (see figure 6(c)) confirms that the all-optical control of the maximum energy electrons is also dominated by the radial fields.



We like to note that all the angular dependent phase offsets in figure 6(c) exhibit a tilt with emission angle. This arises from the change of the relative phase of the two-color field on the nanosphere surface due to field propagation [19]. The relative phase changes only weakly as function of angle on both front side ($\theta_{\text{em}} > 100^{\circ}$) and back side ($\theta_{\text{em}} < 60^{\circ}$) of the nanosphere. In between, in the most relevant ‘hot’ area with strong field enhancement (see figure 1(b)), the phase change has a roughly linear slope and is in good agreement with the evolution of φ_{pot} . Most importantly, the directional switching (see black lines in figure 6(a)) can unambiguously be attributed to the two-color effect on the trajectories.

3. Conclusions

In conclusion, all-optical control of the directional emission of a considerable fraction of the most energetic electrons from nanospheres with intense two-color femtosecond laser fields was demonstrated. The control is observed for nanoparticle sizes for which the Mie size parameter ρ is above unity for at least the 2ω field. Trajectory simulations captured both the two-color phase modulation and optimal emission angles for the energetic photoemission at different ω - 2ω intensity ratios. A selective activation of the 2ω field in the simulations

revealed the pivotal effect of the trajectory modification on the energetic electron emission. The all-optical control scheme demonstrated for isolated nanospheres is expected to be applicable also in more complex (isolated and surface based) nanosystems. The presented work paves the way towards all-optical control of quantum dynamics in near-fields and may find applications in the generation and control of ultrashort electron pulses.

Acknowledgments

We are grateful for support by the Max Planck Society and the DFG through SPP1840 (QUTIF), SFB 652, ZH 582/1–1 and the Cluster of Excellence: Munich-Centre for Advanced Photonics (MAP). AS and MG acknowledge partial support in the frame of the DFG project GA-2169/5-1. TF acknowledges support by a DFG Heisenberg fellowship (FE 1120/4-1). QL, SZ, PR, PW, and MFK acknowledge support from the European Union via the ERC grant ATTOCO (307203). ER is grateful for support by the BMBF (05K16KEA). MFC was supported by the project Advanced research using high intensity laser produced photons and particles (CZ.02.1.01/0.0/0.0/16_019/0000789) from the European Regional Development Fund (ADONIS). SA and DK are grateful for support by NRF funded by the Ministry of Science and ICT (No. 2016K1A4A4A01922028) and KIAT grant funded by the Korean Government (MOTIE) (P0008763, The Competency Development Program for Industry Specialist).

ORCID iDs

Qingcao Liu  <https://orcid.org/0000-0002-3691-7369>
Lennart Seiffert  <https://orcid.org/0000-0002-2389-5295>
Eckart Rühl  <https://orcid.org/0000-0002-0451-8734>
Marcelo F Ciappina  <https://orcid.org/0000-0002-1123-6460>
Markus Gallei  <https://orcid.org/0000-0002-3740-5197>
Thomas Fennel  <https://orcid.org/0000-0002-4149-5164>
Matthias F Kling  <https://orcid.org/0000-0002-1710-0775>

References

- [1] Krausz F and Ivanov M 2009 Attosecond physics *Rev. Mod. Phys.* **81** 163–234
- [2] De S *et al* 2009 Field-free orientation of CO molecules by femtosecond two-color laser fields *Phys. Rev. Lett.* **103** 153002
- [3] Förster M, Paschen T, Krüger M, Lemell C, Wachter G, Libisch F, Madlener T, Burgdörfer J and Hommelhoff P 2016 Two-color coherent control of femtosecond above-threshold photoemission from a tungsten nanopip *Phys. Rev. Lett.* **117** 217601
- [4] Seiffert L, Paschen T, Hommelhoff P and Fennel T 2018 High-order above-threshold photoemission from nanopips controlled with two-color laser fields *J. Phys. B: At. Mol. Opt. Phys.* **51** 134001
- [5] Skruszewicz S, Tiggesbäumker J, Meiwes-Broer K H, Arbeiter M, Fennel T and Bauer D 2015 Two-color strong-field photoelectron spectroscopy and the phase of the phase *Phys. Rev. Lett.* **115** 043001
- [6] Eicke N and Lein M 2017 Extracting trajectory information from two-color strong-field ionization *J. Mod. Opt.* **64** 981–6
- [7] Stefanie K, Dominik P, Daniela J, Lars E, Tim B and Matthias W 2017 Control of photoelectron momentum distributions by bichromatic polarization-shaped laser fields *New J. Phys.* **19** 103017
- [8] Shafir D, Mairesse Y, Villeneuve D M, Corkum P B and Dudovich N 2009 Atomic wavefunctions probed through strong-field light-matter interaction *Nat. Phys.* **5** 412
- [9] Lin K *et al* 2017 Comparison study of strong-field ionization of molecules and atoms by bicircular two-color femtosecond laser pulses *Phys. Rev. Lett.* **119** 203202
- [10] Gong X *et al* 2017 Energy-resolved ultrashort delays of photoelectron emission clocked by orthogonal two-color laser fields *Phys. Rev. Lett.* **118** 143203
- [11] Dudovich N, Smirnova O, Levesque J, Mairesse Y, Ivanov M Y, Villeneuve D M and Corkum P B 2006 Measuring and controlling the birth of attosecond XUV pulses *Nat. Phys.* **2** 781
- [12] Ray D, Chen Z, De S, Cao W, Litvinyuk I V, Le A T, Lin C D, Kling M F and Cocke C L 2011 Momentum spectra of electrons rescattered from rare-gas targets following their extraction by one- and two-color femtosecond laser pulses *Phys. Rev. A* **83** 013410
- [13] Krausz F and Stockman M I 2014 Attosecond metrology: from electron capture to future signal processing *Nat. Photonics* **8** 205–13
- [14] Kling M F and Vrakking M J J 2008 Attosecond electron dynamics *Annu. Rev. Phys. Chem.* **59** 463–92
- [15] Goulielmakis E, Yakovlev V S, Cavalieri A L, Uiberacker M, Pervak V, Apolonski A, Kienberger R, Kleineberg U and Krausz F 2007 Attosecond control and measurement: lightwave electronics *Science* **317** 769–75
- [16] Ciappina M F *et al* 2017 Attosecond physics at the nanoscale *Rep. Prog. Phys.* **80** 054401
- [17] Seiffert L *et al* 2017 Attosecond chronoscopy of electron scattering in dielectric nanoparticles *Nat. Phys.* **13** 766
- [18] Hommelhoff P and Kling M F (ed) 2015 *Attosecond Nanophysics: From Basic Science to Applications* (New York: Wiley)
- [19] Süßmann F *et al* 2015 Field propagation-induced directionality of carrier-envelope phase-controlled photoemission from nanospheres *Nat. Commun.* **6** 7944
- [20] Liu Q *et al* 2018 Attosecond streaking metrology with isolated nanotargets *J. Opt.* **20** 024002
- [21] Zherebtsov S *et al* 2011 Controlled near-field enhanced electron acceleration from dielectric nanospheres with intense few-cycle laser fields *Nat. Phys.* **7** 656

- [22] Zherebtsov S *et al* 2012 Carrier-envelope phase-tagged imaging of the controlled electron acceleration from SiO₂ nanospheres in intense few-cycle laser fields *New J. Phys.* **14** 075010
- [23] Rupp P *et al* 2016 Quenching of material dependence in few-cycle driven electron acceleration from nanoparticles under many-particle charge interaction *J. Mod. Opt.* **64** 995–1003
- [24] Krüger M, Schenk M and Hommelhoff P 2011 Attosecond control of electrons emitted from a nanoscale metal tip *Nature* **475** 78–81
- [25] Piglosiewicz B, Schmidt S, Park D J, Vogelsang J, Grosz P, Manzoni C, Farinello P, Cerullo G and Lienau C 2014 Carrier-envelope phase effects on the strong-field photoemission of electrons from metallic nanostructures *Nat. Photon.* **8** 37–42
- [26] Chew S H *et al* 2016 Laser intensity effects in carrier-envelope phase-tagged time of flight-photoemission electron microscopy *Appl. Phys. B* **122** 102
- [27] Irvine S E, Dombi P, Farkas G and Elezzabi A Y 2006 Influence of the carrier-envelope phase of few-cycle pulses on ponderomotive surface-plasmon electron acceleration *Phys. Rev. Lett.* **97** 146801
- [28] Rác P, Irvine S E, Lenner M, Mitrofanov A, Baltuška A, Elezzabi A Y and Dombi P 2011 Strong-field plasmonic electron acceleration with few-cycle, phase-stabilized laser pulses *Appl. Phys. Lett.* **98** 111116
- [29] Herink G, Solli D R, Gulde M and Ropers C 2012 Field-driven photoemission from nanostructures quenches the quiver motion *Nature* **483** 190–3
- [30] Wilson K R, Zou S, Shu J, Rühl E, Leone S R, Schatz G C and Ahmed M 2007 Size-dependent angular distributions of low-energy photoelectrons emitted from NaCl nanoparticles *Nano Lett.* **7** 2014–9
- [31] Stöber W, Fink A and Bohn E 1968 Controlled growth of monodisperse silica spheres in the micron size range *J. Colloid Interface Sci.* **26** 62–9
- [32] Graf C and van Blaaderen A 2002 Metallodielectric colloidal core-shell particles for photonic applications *Langmuir* **18** 524–34
- [33] Ahmad I *et al* 2009 Frontend light source for short-pulse pumped OPCPA system *Appl. Phys. B* **97** 529
- [34] Förg B *et al* 2016 Attosecond nanoscale near-field sampling *Nat. Commun.* **7** 11717
- [35] Süßmann F *et al* 2011 Single-shot velocity-map imaging of attosecond light-field control at kilohertz rate *Rev. Sci. Instrum.* **82** 093109
- [36] Passig J *et al* 2017 Nanoplasmonic electron acceleration by attosecond-controlled forward rescattering in silver clusters *Nat. Commun.* **8** 1181
- [37] Seiffert L, Süßmann F, Zherebtsov S, Rupp P, Peltz C, Rühl E, Kling M F and Fennel T 2016 Competition of single and double rescattering in the strong-field photoemission from dielectric nanospheres *Appl. Phys. B* **122** 101
- [38] Hickstein D D *et al* 2012 Direct visualization of laser-driven electron multiple scattering and tunneling distance in strong-field ionization *Phys. Rev. Lett.* **109** 073004
- [39] Paschen T, Förster M, Krüger M, Lemell C, Wachter G, Libisch F, Madlener T, Burgdörfer J and Hommelhoff P 2017 High visibility in two-color above-threshold photoemission from tungsten nanotips in a coherent control scheme *J. Mod. Opt.* **64** 1054–60
- [40] Paulus G G, Nicklich W, Xu H, Lambropoulos P and Walther H 1994 Plateau in above threshold ionization spectra *Phys. Rev. Lett.* **72** 2851–4
- [41] Ammosov M V, Delone N B and Krainov V P 1986 Tunneling ionization of complex atoms and atomic ions in a varying electromagnetic field *Sov. Phys. JETP* **64** 1191–4
- [42] Seiffert L, Henning P, Rupp P, Zherebtsov S, Hommelhoff P, Kling M F and Fennel T 2017 Trapping field assisted backscattering in strong-field photoemission from dielectric nanospheres *J. Mod. Opt.* **64** 1096–103